Adaptive analytical mapping procedure for efficiently solving the radial Schrödinger equation

Vladimir V. Meshkov,[1] Andrey V. Stolyarov,[1,2,*] and Robert J. Le Roy[2]
[1]*Department of Chemistry, Moscow State University, 119992 Moscow, Russia*
[2]*Guelph-Waterloo Center for Graduate Work in Chemistry and Biochemistry, University of Waterloo, Waterloo, Ontario N2L 3G1, Canada*
(Received 17 July 2008; published 19 November 2008)

This paper shows that replacing the usual integration variable $r \in [0,\infty)$ by a reduced radial variable $y \equiv y(r;\vec{\alpha})$ defined analytically on a finite domain $y \in [a,b]$ transforms the conventional radial Schrödinger equation into an equivalent form in which treatment of levels lying extremely close to dissociation becomes just as straightforward and routine as treating levels in the lower part of the potential well. Explicit integral expressions for the eigenvalue error due to the use of a finite step size in finite-difference methods of numerical integration are presented and are used to improve calculated eigenvalues as well as to determine optimal values of the mapping parameters $\vec{\alpha}$. This adaptive mapping procedure is shown to be versatile and efficient for both finite-difference and pseudospectral methods.

DOI: 10.1103/PhysRevA.78.052510 PACS number(s): 31.15.−p, 33.15.Mt

I. INTRODUCTION

Solutions of the familiar radial or effective one-dimensional Schrödinger equation

$$\frac{d^2\psi(r)}{dr^2} = -Q(E;r)\psi(r) \equiv -\left\{\frac{2\mu}{\hbar^2}[E-U(r)]\right\}\psi(r) \quad (1)$$

defined on the infinite domain $r \in [0,\infty)$ are often required for adiabatic modeling and simulations of a wide variety of experimental phenomena. For example, analysis of photoassociation experiments, prediction of formation rates for ultracold molecules, and determination of scattering lengths and collision cross sections at very low temperatures all require highly accurate quantum calculations based on numerical solution of this equation. Furthermore, modern direct-potential-fit (DPF) analyses of diatomic molecule spectroscopic data must solve Eq. (1) to high accuracy for the upper and lower levels of thousands or tens of thousands spectroscopic transitions in each cycle of the nonlinear least-squares fit which optimizes the parameters defining the upper and lower-state potential energy functions [1–5]. Thus it is important that the method used for solving this equation be robust, accurate, and as efficient as possible. For levels lying in the lower part of the well where the potential function is only modestly asymmetric, a wide variety of algebraic, basis-set, or wave-function propagation methods can satisfy this need. However, studies of ultracold atomic and molecular systems often involve very weakly bound levels which lie extremely close to dissociation and have outer turning points of tens, hundreds, or thousands of Å. Performing accurate calculations of the energies and other properties of such levels from a given potential energy function using conventional methods can be quite challenging.

The nature of the problem is illustrated by Fig. 1 which shows the wave functions $\psi_v(r)$ for a range of vibrational levels v of a model Lennard-Jones $(2n,n)$ potential

$$U_{\mathrm{LJ}}^{2n,n}(r) = \mathfrak{D}_e\left[\left(\frac{r_e}{r}\right)^{2n} - 2\left(\frac{r_e}{r}\right)^{n}\right] \quad (2)$$

with $n=4$, in which $\mathfrak{D}_e$ is the well depth and r_e is the equilibrium internuclear distance, and the wave functions satisfy the usual boundary and normalization conditions

$$\psi_v(0) = \psi_v(\infty) = 0; \quad \int_0^\infty |\psi_v(r)|^2 dr = 1. \quad (3)$$

The very different magnitudes of the intervals spanned by the wave functions for different levels, the fact that a loga-

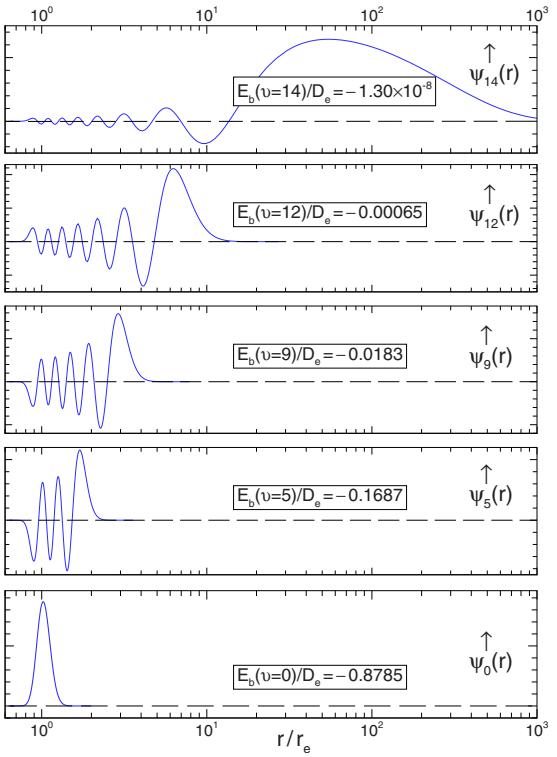

FIG. 1. (Color online) Radial eigenfunctions $\psi_v(r)$ of the model 15-level LJ (8,4) potential of Table I.

*Corresponding author. avstol@phys.chem.msu.ru

rithmic scale is required to show the entire wave functions for the higher levels, and the great differences in their amplitudes and peak widths in the inner and outer turning-point region present considerable challenges to most methods. In particular, the robust and efficient finite-difference [6–13] and pseudospectral collocation [14–21] methods which exploit grids of equidistant r points are not well suited for this type of molecular boundary value problems.

A grid mapping procedure based on an adaptive radial coordinate $y(r)$ has been proposed as an efficient tool for addressing this type of problem [16–21]. The numerically defined mapping function

$$y(r) \sim \int_{r_0}^{r} \sqrt{Q(E;r)}dr; \quad Q(E;r) \geqslant 0 \tag{4}$$

was assumed to be optimal for the Fourier grid Hamiltonian (FGH) method in the classical allowed region where $Q(E;r)>0$. A nontrivial scheme for improving the above mapping near the classical turning points was suggested in Ref. [19]. However, artifacts related to the appearance of spurious (*ghost*) states in the mapped FGH method have been associated with this approach [18,21].

The present work presents an alternate mapping procedure designed to provide efficient solutions of Eq. (1) for very weakly bound levels. The key to this approach is replacement of the usual integration variable $r \in [0,\infty)$ by a reduced radial variable which is defined on a *finite* domain $y \in [a,b]$ and has an *analytical* form written formally as $y \equiv y(r;\vec{\alpha})$. This approach achieves considerable economy with regard to computational effort and array storage requirements for both finite-difference and pseudospectral methods of solving Eq. (1). More importantly, it makes the treatment of levels lying extremely close to dissociation just as straightforward as performing calculations for those lying deep in the well.

Ascertaining the accuracy of calculations for levels lying extremely near dissociation can also be a challenging problem. To address this question, an integral expression for estimating the residual error associated with use of a finite radial mesh size in solving our transformed radial Schrödinger equation is derived and used to examine the effect of different choices of the parameters $\vec{\alpha}$ governing the mapping of the conventional radial variable r onto a finite domain.

II. METHODOLOGY

A. The coordinate transformation

On introducing a new radial coordinate function $y(r)$ which is a smooth, monotonically increasing function of r, our initial radial equation (1) becomes

$$\left[\frac{d^2}{dy^2} - \left(\frac{g'}{g}\right)\frac{d}{dy} + g^2 Q\right]\psi = 0 \tag{5}$$

in which

$$g(y) \equiv \frac{dr(y)}{dy} = 1 \Big/ \frac{dy(r)}{dr} > 0 \tag{6}$$

and $r(y)$ is defined on the interval $y \in [a,b]$ as the inverse function of $y(r)$, while a prime ($'$) denotes differentiation with respect to the new variable y. The substitution

$$\psi(r) = \sqrt{g}\phi(y) \tag{7}$$

then transforms Eq. (5) into the conventional form

$$\frac{d^2\phi(y)}{dy^2} = -\tilde{Q}(E;y)\phi(y) \tag{8}$$

in which

$$\tilde{Q}(E;y) \equiv g^2(y)Q(E;r(y)) + F(y) \tag{9}$$

and the additive term

$$F(y) = \frac{g''}{2g} - \frac{3}{4}\left(\frac{g'}{g}\right)^2 \tag{10}$$

depends only on the definition of the new radial coordinate. Equation (8) may also be rewritten in the equivalent form

$$\left[-\frac{\hbar^2}{2\mu}\frac{d^2}{dy^2} + g^2\tilde{U}\right]\phi = g^2 E\phi \tag{11}$$

in which

$$\tilde{U} \equiv U - \frac{\hbar^2}{2\mu}\frac{F(y)}{g(y)^2} \tag{12}$$

is the effective potential.

When combined with the modified boundary and normalization conditions

$$\phi(a) = \phi(b) = 0; \quad \int_a^b |g(y)\phi(y)|^2 dy = 1 \tag{13}$$

Eqs. (8) and (11) are completely equivalent to the initial equation (1) as long as $r(y) \in C^3([a,b])$ is a monotonically increasing function. It should be stressed that only the inverse function $r(y)$ is needed to accomplish the analytical transformations of the initial equation (1).

We note that combination of the mapping function of Eq. (4) with the substitution of Eq. (7) actually corresponds to the well-known Liouville-Green transformation [22] which leads to the conventional WKB approximation [23,24]. Indeed, the substitution $g(y)=dr/dy=1/p$ [where $p \equiv \sqrt{Q(E;r)}$ is the classical impulse] transforms Eq. (8) to the form

$$\frac{d^2\phi}{dy^2} = -[1 + F(y)]\phi \tag{14}$$

in which the function $F(y) \approx 0$ when $p \gg 0$, in which case

$$\phi(y) \approx C_1 \sin(y) + C_2 \cos(y), \tag{15}$$

$$\psi(r) \approx \frac{C_1}{\sqrt{p}} \sin\left(\int p dr\right) + \frac{C_2}{\sqrt{p}} \cos\left(\int p dr\right). \quad (16)$$

Thus, recovery of the semiclassical results of Eqs. (15) and (16) justifies the argument that the mapping (4) could be optimal for the Fourier grid methods of solution. However, Eq. (4) cannot be applied straightforwardly to define a mapping function on a whole domain, since Eq. (15) is only valid deep inside the classical allowed region.

B. Solution of the transformed equations

Equation (8) is linear homogeneous differential equation whose solutions are oscillating sinusoidal functions in the pseudoclassical region where $\tilde{Q}(E;y)$ is positive, and decay exponentially in the boundary regions where it is negative. Any direct integration scheme can straightforwardly be applied to solve Eq. (8) using a "shooting" propagation method [13]. In particular, simply replacing $Q(E;r)$ by $\tilde{Q}(E;y)$ transforms a code which uses the Numerov integration scheme [6–9] to solve Eq. (1) [25] into a code for solving Eq. (8). The only other modification required is the replacement of the conventional normalization conditions of Eq. (3) by those of Eq. (13). In particular, the Löwdin-Cooley eigenvalue correction $\delta(E)$ [6,8] becomes

$$\delta(E) = \frac{(-\tilde{Y}_{M-1} - \tilde{Y}_{M+1} + 2\tilde{Y}_M)/h^2 - \tilde{Q}_M \phi_M}{\Sigma_{i=1}^{N} |\phi_i g_i|^2} \quad (17)$$

in which $\tilde{Y}_i = [1 + (h^2/12)\tilde{Q}_i]\phi_i$, M is the wave-function array matching mesh point, $h=(b-a)/(N-1)$ is the integration step [26], and N is the total number of uniformly spaced grid points. Furthermore, in any calculation of matrix elements using the eigenfunctions $\phi(y)$, the integrand must include the weight function $g^2(y)$:

$$M_{ij} \equiv \int_0^\infty \psi_i(r) M(r) \psi_j(r) dr = \int_a^b \phi_i(y) M[r(y)] \phi_j(y) g(y)^2 dy. \quad (18)$$

The matrix realization of the most robust and efficient finite-difference and pseudospectral methods of numerical integration reduces the transformed equation (11) to the generalized eigenvalue problem

$$\mathbf{A}\phi = \tilde{E}\mathbf{B}\phi, \quad (19)$$

where $\mathbf{A}$ is a symmetric (and for finite difference methods, banded) matrix, while $\mathbf{B}$ is a positive definite diagonal matrix with elements $B_{ii}=g_i^2$. The substitution

$$\phi = \mathbf{B}^{-1/2}\varphi \quad (20)$$

based on the trivial matrix decomposition $\mathbf{B}=\mathbf{B}^{1/2}\mathbf{B}^{1/2}$ then yields the ordinary eigenvalue problem:

$$[\mathbf{B}^{-1/2}\mathbf{A}\mathbf{B}^{-1/2}]\varphi = \tilde{E}\varphi; \quad \varphi(a) = \varphi(b) = 0, \quad (21)$$

where the wave function $\varphi(y)$ satisfies the standard normalization condition $\int_a^b |\varphi(y)|^2 dy = 1$, and hence $M_{ij} = \int_a^b \varphi_i M[r(y)] \varphi_j dy$.

C. Minimizing eigenvalue error

For nonsingular potential energy functions whose eigenfunctions satisfy the boundary conditions of Eq. (13), the perturbative arguments given in Appendix A provide an elegant means of estimating the eigenvalue error ΔE associated with use of a finite step size h. In particular, for a central three-point finite difference scheme (FD3), the error is given by the integral

$$\Delta E_{\mathrm{FD3}}(h) = \frac{\hbar^2}{2\mu}\left(\frac{h^2}{12}\right)\int_a^b [\tilde{Q}\phi]^2 dy \quad (22)$$

while for the Numerov integration method (Num), which is subject to the additional boundary condition

$$\phi'(a) = \phi'(b) = 0, \quad (23)$$

the error term is

$$\Delta E_{\mathrm{Num}}(h) = \frac{\hbar^2}{2\mu}\left(\frac{h^4}{240}\right)\int_a^b \left[\frac{d(\tilde{Q}\phi)}{dy}\right]^2 dy. \quad (24)$$

These expressions indicate that in contrast to variational methods, for small h the FD3 and Numerov methods give *lower* bounds to the exact eigenvalues for bound levels of Eqs. (1) and (8), as had been discovered empirically by Shore [12]. However, for cases in which some other boundary condition is appropriate, such as for quasibound levels or for a model potential which is a singular function at one end of the range, the more general energy correction formulas given in Appendix A should be used.

In practice, the asymmetry of typical interatomic potentials means that the limiting region where $r \to 0$ (or $y \to a$) is completely inaccessible. As a result, for both FD3 and Numerov methods it is customary to define the inner boundary condition as a node at some moderately small distance r_a, where $0 < r_a < r_e$. As long as the exponentially decreased wave-function amplitude approaching this node is several orders of magnitude smaller (e.g., by a factor of 10^{-9}) than that in the classically allowed region, the precise location of this inner starting point is immaterial, and the boundary condition on the first derivative of the wave function (23) is effectively fulfilled at the selected point r_a or $y(r_a)$. Analogous considerations apply to the treatment of the outer boundary for strongly bound levels of "well-behaved" potentials, although for levels lying very near dissociation, the outer boundary condition must be applied at the upper bound $y=b$, and limitations arise regarding suitable values of the parameters $\vec{\alpha}$ defining the mapping function (see Sec. III).

The practical value of a particular coordinate mapping procedure will depend (i) on its ability to treat all cases of interest, and (ii) on a minimization of the computational effort (CPU time and memory) required to solve the modified equation (8). For grid methods, the latter consideration implies a minimization of the total number of mesh points N required to yield solutions with a given level of accuracy, since the computational effort scales roughly as N. In general, the choice of an optimal mapping function will depend simultaneously on the nature of the potential, on the energy region of interest, and on the particular numerical method

used. However, numerical tests showed that the choice of optimum mapping parameters $\vec{\alpha}$ were not strongly dependent on the mesh size h (or total array size N), so most tests reported below were performed by varying $\vec{\alpha}$ with the mesh size fixed. Thus for bound states with conventional boundary conditions, the optimal mapping parameters can be found by minimizing the eigenvalue error estimates given by Eq. (22) for an FD3 procedure, or by Eq. (24) if a Numerov procedure is being used. Expressed in terms of the eigenfunctions obtained at some constant mesh, this corresponds to the minimizations

$$\min_{\vec{\alpha}}\left\{h^3\sum_{i=1}^{N}[\tilde{Q}_i\phi_i]^2\right\} \tag{25}$$

and

$$\min_{\vec{\alpha}}\left\{h^3\sum_{i=1}^{N-1}[\tilde{Q}_{i+1}\phi_{i+1}-\tilde{Q}_{i-1}\phi_{i-1}]^2\right\}, \tag{26}$$

respectively, for a given fixed N (or fixed h) value.

While explicit expressions for the energy truncation error are not available for collocation methods, the optimal mapping parameters can be found by minimizing the last few coefficients of the spectral expansion of the wave function [20] with respect to $\vec{\alpha}$, because the spectral series is accurate if the magnitudes of the coefficients decrease rapidly. This more qualitative minimization procedure is required for the collocation method since the calculated eigenvalues $E_{N_{\rm coll}}$ do not converge monotonically to $E_{N_{\rm coll}\to\infty}$ as the number of collocation points increases, and local oscillations of the difference $|E_{N_{\rm coll}}-E_{N_{\rm coll}\to\infty}|$ can occur (see Sec. IV).

Equations (22) and (24) also show how eigenvalue convergence error depends on the integration step size h. However, to facilitate the choice of an appropriate value of h for any particular problem, it is useful to convert these results to an (approximate) alternate form. Consider the Numerov integration case of Eq. (24). In the classically allowed region where $\tilde{Q}>0$ one can approximate the wave function by the semiclassical expression $\varphi(y)\approx(C/\tilde{Q}^{1/4})\sin(\int\tilde{Q}^{1/2}dy+\eta)$ and we may divide the interval $[a,b]$ into subintervals each corresponding to one "loop" of the semiclassical wave function. Assuming that $\tilde{Q}$ is approximately constant across a given subinterval, its length will be equal to $\pi/\tilde{Q}^{1/2}$. The number of mesh points N_ℓ on the subinterval associated with that "loop" of the wave function is then $\pi/(\tilde{Q}^{1/2}h)$, and the contribution to the eigenvalue error associated with this wave-function loop is

$$\Delta E_{\rm Num}^{\rm loop}\approx\pi\frac{\hbar^2}{2\mu}\left(\frac{C^2h^4}{480}\right)\tilde{Q}^2\approx\frac{\hbar^2}{2\mu}\left(\frac{C^2\pi^5}{480}\right)\frac{1}{(N_\ell)^4}. \tag{27}$$

The total error would be a sum of such terms, the largest of which would arise from the interval on which N_ℓ is smallest (i.e., on which $\tilde{Q}$ is largest). Thus it seems reasonable to characterize the level of accuracy in a given case by the smallest value of N_ℓ for its wave function, which implies that the integration mesh size for a given system may be defined as

$$h=\frac{\pi}{(\tilde{Q}_{\rm max}^{1/2}N_\ell)}\approx\frac{\pi\sqrt{\hbar^2/2\mu}}{\sqrt{\max\{g(y)^2[E-U(r)]\}}}\frac{1}{N_\ell}$$
$$\approx\sqrt{\frac{\hbar^2}{2\mu\mathfrak{D}_e}}\frac{\pi}{g(r_e)N_\ell}. \tag{28}$$

Experience indicates that using this definition and $N_\ell\gtrsim 30$ gives realistic results for most cases, while higher accuracy is achieved readily, since the errors decrease by a factor of 2^4 for each doubling of N_ℓ.

Note, however, that for numerical round-off reasons, defining the binding energy of the very highest level even to only one or two significant digits will tend to require a higher degree of absolute accuracy than would normally be required to provide satisfactory precision for the lower levels. Thus accurately describing extremely weakly bound levels may require a somewhat finer mesh than would be needed to give satisfactory results for the lower levels.

III. REDUCED VARIABLE MAPPING

It is now necessary to introduce an explicit definition for the new radial variable $y(r)$. A particularly convenient choice is a two-parameter version of the Šurkus variable [27], which is also proving to be useful in representing potential energy functions [28–31]:

$$y(r;\alpha,\bar{r}>0)=\frac{(r/\bar{r})^\alpha-1}{(r/\bar{r})^\alpha+1};\quad y\in[-1,1] \tag{29}$$

or

$$r(y)=\bar{r}\left(\frac{1+y}{1-y}\right)^{1/\alpha}. \tag{30}$$

For this case

$$g(y)\equiv\frac{dr(y)}{dy}=\frac{2\bar{r}}{\alpha}\frac{(1+y)^{1/\alpha-1}}{(1-y)^{1/\alpha+1}}=\frac{(r^\alpha+\bar{r}^\alpha)^2}{2\alpha\bar{r}^\alpha r^{\alpha-1}} \tag{31}$$

and the function $F(y)$ of Eq. (10) has the form

$$F(y)=\frac{1-1/\alpha^2}{(1-y^2)^2}. \tag{32}$$

Many other choices for the definition of the transformed variable are possible [32]. However, the present paper focuses on the use of Eq. (29) because the analytic simplicity of Eqs. (29)–(32) makes it particularly easy to use and facilitates making optimum choices for the mapping function parameters (see below). In any case, since they map the infinite interval of the initial radial coordinate $r\in[0,\infty)$ onto a finite domain, all of these mapping functions avoid the type of "termination" errors [12] associated with truncation of the integration range, a problem which can be especially problematic for the levels lying closest to the dissociation limit. Note that the transformation of Eq. (1) into Eq. (8) using the variable mapping of Eq. (29) is an exact procedure, because

TABLE I. Properties of selected model LJ $(2n,n)$ potentials, with lengths in Å and energies in cm^{-1}. All models have equilibrium distance $r_e=1$ Å, and the reduced mass is set as $\mu=16.857\,629\,20$ au so that in "spectroscopists units," the scaling factor $\hbar^2/(2\mu)=1\ cm^{-1}\ Å^2$.

n	v_{last}	$\mathfrak{D}_e$	$\mathfrak{D}_e-E(0)$	$\mathfrak{D}_e-E(v_{last})$	$r_{max}(v_{last})$
6	14	3761	3403.4732790098	$1.79465837533\times10^{-5}$	27.4
5	14	2165	1939.7924547397	$1.81287028897\times10^{-5}$	47.4
4	14	1000	878.45204473428	$1.29964564537\times10^{-5}$	111.4
3	14	270	223.64254525927	$1.55428504268\times10^{-7}$	1514.6
3	300	107000	106021.67122428	$1.5738671521\times10^{-13}$	1107852.

the required $g(y)$ and $F(y)$ functions are unambiguously defined as analytic functions on the whole domain.

At sufficiently long range, all attractive intermolecular potentials take on the limiting behavior $U(r)\simeq\mathfrak{D}-C_n/r^n$, where $\mathfrak{D}$ is the energy at the asymptote, the power n is an integer determined by the nature of the dissociating atomic fragments [33–35], and the constant C_n may often be calculated from theory. If we ignore the special case of ion-pair states, the limiting value of n is always one of $n=6$, 5, 4, or 3 [36–38]. The utility and limitations of the proposed mapping procedure are therefore illustrated by examining its application to a set of 15-level LJ $(2n,n)$ model potentials (2) for $n=3$, 4, 5, and 6, whose well depths were adjusted to ensure that the highest level is very weakly bound. Parameters defining the selected LJ $(2n,n)$ potentials are given in Table I.

For the same model LJ (8,4) potential considered in Fig. 1, results obtained on solving Eq. (8) in terms of the mapping variable of Eq. (29) for $\alpha=1$ (and $\bar{r}=r_e=1$ Å) are seen in Fig. 2. The differences between the nature of the wave functions seen in Figs. 1 and 2 illustrate the essential advantages of the present procedure. While the wave functions $\psi_v(r)$ are spread asymmetrically across an immense domain and have amplitudes and node spacings which vary dramatically across that range, all the eigenfunctions $\phi_v(y)$ of Eq. (8) are restricted to the same finite domain $y\in[-1,1]$, and the node spacings and loop amplitudes change relatively little between the turning points of a given level. This approximate constancy of node spacings means that for fixed-mesh computational methods, a given mesh size will give rise to approximately the same values of N_ℓ, and hence approximately the same contribution to the eigenvalue error, for all loops of that wave function. This means that a much smaller total number of mesh points N will be required to yield a given level of accuracy for all levels of a given potential, which in turn means that much less computational effort and array storage will be required than with conventional treatments which use r as the radial variable.

While the illustrative results seen in Fig. 2 are very promising, care must be taken with choice of the mapping function parameters α and $\bar{r}$ of Eq. (29). For a fixed mesh of equally spaced points on the interval $y\in[-1,1]$, the density distribution function for those mesh points as a function of r is $\rho(r)=A(dy/dr)=A/g(r)$, where A is a normalization factor. The plots of these distribution functions shown in Fig. 3 indicate that for most cases, the mesh point density is fairly close to its maximum for $r\approx\bar{r}$. However, the discussion of Sec. II C shows that to minimize eigenvalue error, the mesh-point density should be highest near the equilibrium internuclear distance where $[E-U(r)]$ is largest. Moreover, numerical tests show that the stability and efficiency of solving Eq. (8) for highly excited states is not very sensitive to the choice of the reference distance $\bar{r}$ in Eq. (29). Hence in the studies reported below $\bar{r}$ is fixed at the equilibrium distance for our various model potentials: $\bar{r}\equiv r_e$.

For the mapping parameter α of Eq. (29), one possible approach would be to use the error minimization procedure of Eqs. (25) or (26) to determine an optimum value α_{opt} for each bound level of interest. Results obtained in this way on applying the Numerov wave-function propagation approach to the 15-level model LJ $(2n,n)$ potentials of Table I are

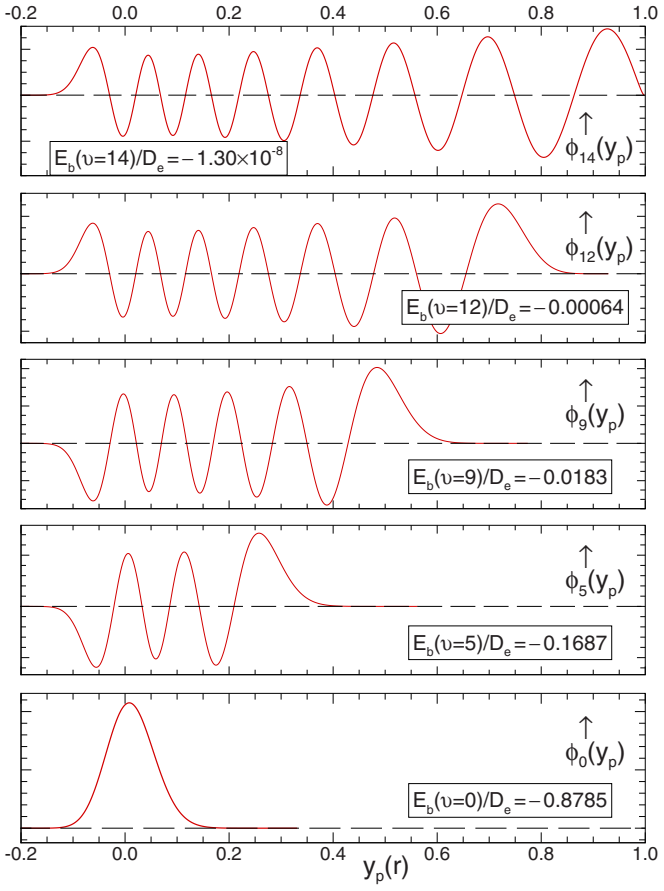

FIG. 2. (Color online) Radial eigenfunctions $\phi_v(y;\alpha=1)$ for the same five levels of the model LJ (8,4) potential considered in Fig. 1.

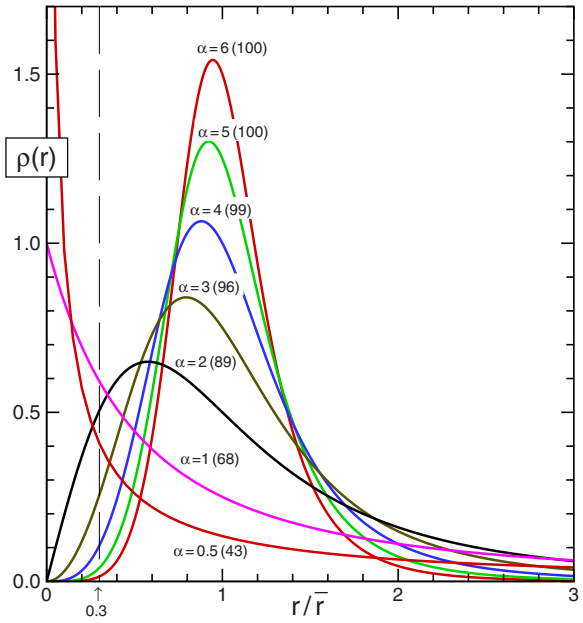

FIG. 3. (Color online) Unit normalized mesh-point (in y) density distribution functions $\rho(r)$ for the mapping function $y(r;\alpha,\bar{r}=r_e=1\ [\text{Å}])$ of Eq. (29) for different values of α. Numbers in brackets denote the percent of the grid points on the interval $[0.3,\infty)$ which are located in the subinterval $r/\bar{r}\in[0.3,3]$ [i.e., the number $100\times\int_{0.3}^{3}\rho(r)dr/\int_{0.3}^{\infty}\rho(r)dr$].

shown in Fig. 4 (use of FD3 methods yields very similar results). However, performing an independent minimization for each level of interest would itself require considerable computational effort and would be counterproductive, as in practical applications it is highly desirable to have all eigenfunctions of a given potential defined in terms of the same

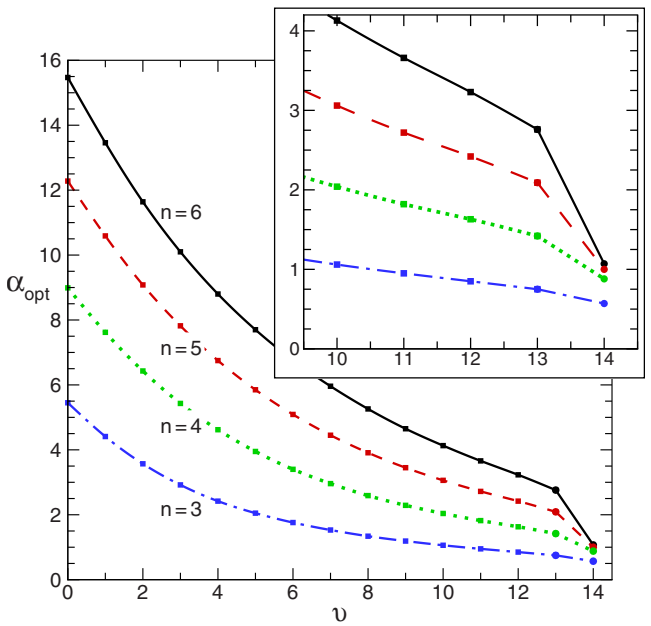

FIG. 4. (Color online) Optimal mapping parameters α for all vibrational levels of our model 15-levels LJ $(2n,n)$ potentials for $n\in\{3,4,5,6\}$ associated with use of the Numerov propagation (Num) method of integration.

radial variable and on the same radial grid. Fortunately, in practice it is usually sufficient to optimize the mapping parameters only for highest energy level of interest, since all lower levels can be calculated efficiently and accurately using that same scheme.

The greatest advantage of our variable mapping procedure is the fact that (see Fig. 2) for small values of α, the description of levels lying very near dissociation becomes qualitatively very similar to that for those deeper in the well. For those very weakly bound levels, $[E-U(r)]\approx[\mathfrak{D}-U(r)]\approx C_n/r^n$ over most of the classically allowed region. Moreover, at these large distances the Jacobian factor of Eq. (31) takes on the behavior $g(y)\simeq r^{\alpha+1}/(2\alpha\bar{r}^{\alpha})$. As a result, if we overlook the additive transformation factor $F(y)$, over much of the domain on which the wave function has significant amplitude, the function $\tilde{Q}(E,y)$ in Eq. (8) behaves as

$$\tilde{Q}(E;r)\approx\frac{2\mu}{\hbar^2}\left(\frac{r^{\alpha+1}}{2\alpha\bar{r}^{\alpha}}\right)^2\frac{C_n}{r^n}=\frac{2\mu}{\hbar^2}\left(\frac{C_n}{4\alpha^2\bar{r}^{2\alpha}}\right)r^{2\alpha+2-n}. \quad (33)$$

Thus if $\alpha=(n/2)-1$ the factor $\tilde{Q}(E;r)$, and hence also the wavefunction node spacings, would be approximately constant over much of the classically allowed region. This is the reason that, except for the very last level, the α_{opt} plots in Fig. 4 tend to approach limiting values of $\alpha_{\text{opt}}=2$, 1.5, 1, and 0.5 for $n=6$, 5, 4, and 3, respectively, for levels approaching dissociation. This suggests that $\alpha=(n/2)-1$ would be an appropriate general rule to govern the selection of mapping function parameter α for a given potential energy function.

The one remaining question concerns the treatment of the very highest, most weakly bound level for each case. The numerical results of Fig. 4 clearly show that for $n=4-6$, the optimum α value for this very last level drops significantly below the trend associated with the other levels, and further tests show that the value of $\alpha_{\text{opt}}(v_{\text{last}})$ for that highest level also depends on the magnitude of its binding energy.

It turns out that this abrupt dropoff of α_{opt} is explained by the behavior of the factor $\tilde{Q}(E;y)$ in the region close to $y=1$ where the approximations which gave rise to Eq. (33) are no longer valid. In particular, because of its singular behavior as $y\to1$ [see Eq. (32)], the contribution of $F(y)$ cannot be ignored. Moreover, at distances well past the outer classical turning point, $[E-U(r)]\simeq-[\mathfrak{D}-E]$, and on taking account of the limiting behavior of $g(y)$ (see above), we find that the "curvature factor" in our differential equation (8) becomes

$$\tilde{Q}(E;y)\simeq-\left\{\frac{2\mu}{\hbar^2}\left(\frac{2\bar{r}}{\alpha}\right)^2[\mathfrak{D}-E]\right\}\frac{(1+y)^{(2/\alpha)-2}}{(1-y)^{(2/\alpha)+2}}+\frac{1-1/\alpha^2}{(1-y^2)^2}. \quad (34)$$

Thus while generally well behaved in the region between the turning points, at y values close to 1 this curvature factor becomes a sum of two terms which both become singular at $y=1$, and which have different mathematical signs for $\alpha>1$. In the limit, the negative singularity of the first term is stronger by the factor $(1-y)^{-2/\alpha}$. However, over much of the region past the outer classical turning point, for $\alpha>1$ the additive $F(y)$ term with its positive singularity is the larger, so $\tilde{Q}(E;y)$ will remain positive almost all the way to $y=1$

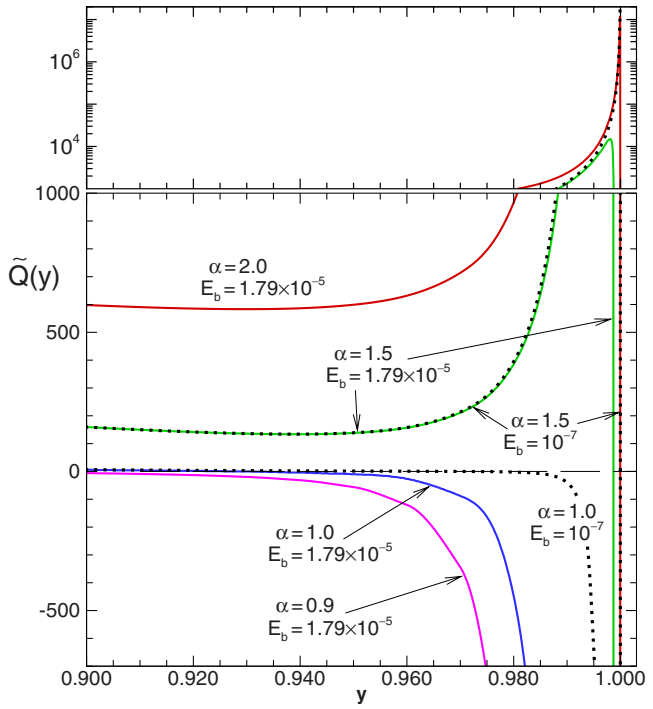

FIG. 5. (Color online) Differential equation curvature factor $\tilde{Q}(E;r)$ for energies very near the dissociation limit of the model LJ (12,6) potential of Table I for different choices of the mapping variable parameter α. Solid curves are for the very highest ($v=14$) bound level of the model potential of Table I; dotted curves are for a hypothetical binding energy of 10^{-7} cm^{-1}.

before it finally changes sign. For the highest bound level of our model LJ (12,6) potential, this behavior is illustrated by the solid curves in Fig. 5. As a result, for $\alpha>1$ $\phi_v(y)$ will be an oscillatory function with substantial amplitude almost all the way to the $y=1$ limit. However, since $g(y)$ also becomes singular as $y\to1$, Eqs. (22) and (24) show than unless the integration mesh h is made extremely small, this interval will make a very large contribution to the overall eigenvalue error. This explains why the values of $\alpha_{\rm opt}$ in Fig. 4 all drop to $\lesssim1$ for the very last bound level of all four model potentials (see below).

When $\alpha=1$ the $F(y)$ term disappears and we are left with only the negative contribution to Eq. (34) near $y=1$. However, this alone may not completely resolve the problem, since the range of y over which $\phi(y)$ has positive curvature (and hence dies off exponentially) may be very narrow, and the very rapid growth of $g(y)^2$ in this region [where it varies as $(1-y)^{2+2\alpha}$] will again give rise to large contributions to the error predicted by Eqs. (24) and (24) unless h is made extremely small. This problem is illustrated by the fact that the positive-curvature exponential die-off of $\phi_{14}(y)$ as $y\to1$ is barely discernable in Fig. 2. On the other hand, if α is given a value slightly less than 1 (say, $\alpha=0.9$), the additive (and singular) $F(y)$ term is also negative, and it makes the curvature factor $\tilde{Q}(E;y)$ large and negative over a much broader region. As a result, the exponential die-off of $\phi_v(y)^2$ will overwhelm the inverse-power growth of $g(y)$ as $y\to1$, and the associated contributions to the error term represented by Eqs. (22) or (24) will be very small. A simple practical test for this condition is whether on propagating $\phi_v(y)$ inward from the outer boundary at $y=1$, the amplitude of $\phi_v(y)$ grows by the same type of factor (say, 10^9) typically associated with the inner boundary condition at r_a (where $0<r_a<r_e$).

In summary therefore the basic approach to solving the radial or one-dimensional Schrödinger equation using Eqs. (8) and (29) using a Löwdin-Cooley type wave-function propagator approach is as follows. The outward wave-function propagation starts from a node set at a value of y corresponding to a distance r_a lying between $r=0$ and r_e which is selected in the usual way (typically, $r_a/r_e\sim0.3-0.6$). The inward wave-function propagation then starts from a node placed exactly at $y=1$ (i.e., at $r\to\infty$), and the correction to the trial energy is calculated in the usual way using Eq. (17). We suggest that a reasonable zeroth order choice for the parameter defining our new radial variable is $\alpha=\frac{n}{2}-1$, where n is the (inverse) power associated with the asymptotic behavior of the potential energy function. For the very last level, setting α slightly smaller than 1 should give good results for $n=6$, 5, and 4, while 0.5 should always suffice for potentials for which $n=3$.

IV. DISCUSSION AND CONCLUSIONS

Most of the preceding discussion focused on application of our mapping procedure in the framework of either a direct wave-function propagation (or "shooting") method based on the Numerov finite-difference integration scheme combined with the Löwdin-Cooley eigenvalue corrector (17), or on straightforward finite-difference methods based on a matrix realization of a central three-points integration scheme (FD3). However, this mapping procedure also allows one to minimize the number of grid points $N_{\rm coll}$ required to achieve convergence when using *pseudospectral* techniques such as Fourier, polynomial, or sinc collocation methods (FCM, PCM, and SCM) [40]. For example, for the very highest level of the 301-level LJ (6,3) potential of Table I [$E_b(300)=1.57\times10^{-13}$ cm^{-1}], Fig. 6 shows how the error in the relative binding energy

$$\delta_v \equiv \left| \frac{E_b(v)}{E_b^{\rm exact}(v)} - 1 \right| \tag{35}$$

depends on the number of collocation points $N_{\rm coll}$ for a range of values of α, for both the polynomial (PCM) and Fourier (FCM) collocation methods. (Here, $E_b^{\rm exact}$ was determined by increasing $N_{\rm coll}$ to attain full convergence.) Collocation method calculations for this level using the conventional radial variable r would be virtually unthinkable because of the immense range involved (see Table I). Figure 6 shows that although the eigenvalue convergence is not simply monotonic (see discussion of Sec. II C), collocation techniques can attain very high accuracy using a very modest number of points, even for this very extreme case. On the basis of the behavior of these plots, we would choose $\alpha_{\rm opt}=0.49$ and 0.31, respectively, for PCM and FCM treatments of this level. In general, the Fourier and Sinc methods yield almost identical results, while PCM allows one to obtain equivalent

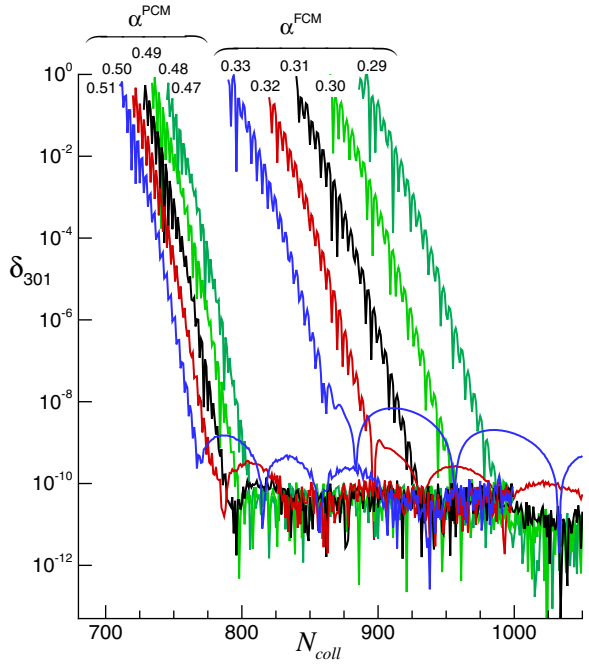

FIG. 6. (Color online) Convergence tests for polynomial (PCM) and Fourier (FCM) collocation method calculations of the binding energy of the very highest level of the 301-level LJ (6,3) potential of Table I.

results with a slightly smaller number of collocation points.

An important advantage of using the Numerov propagation method for solving the radial Schrödinger equation is the ability to locate quasibound (or tunneling-predissociation) levels which lie above the asymptote but below a potential energy maximum barrier, by applying an Airy-function outer boundary condition at the outermost turning point [25,42,43]. Fortunately, it is a straightforward matter to combine that definition of the outer boundary condition with the use of Eq. (8). Thus, this automatic and highly efficient method of locating such metastable levels is retained on replacing the conventional Schrödinger equation in r of Eq. (1) by our Schrödinger equation in y, Eq. (8). Similarly, Eq. (18) shows that Franck-Condon factors and other matrix elements may be routinely generated in the new scheme, and a straightforward extension of this approach to inhomogeneous versions of Eqs. (1) and (8) allows the calculation of diatomic molecule centrifugal distortion constants using the exact quantum mechanical method of Hutson [44]. Moreover, while the above discussion has focused on rotationless vibrational levels, incorporating the repulsive centrifugal distortion term $J(J+1)/2\mu r^2$ due to molecular rotation into the effective potential raises no challenges. A version of the widely used LEVEL program [25] based on the present method will be released shortly.

Another useful result presented herein is the integral expressions of Eqs. (22) and (24) for predicting the residual eigenvalue error associated with a given finite-mesh propagation or three-point finite-difference calculation. As an illustrative test of these expressions, Table II compares the relative error δ_v in the eigenvalue of the the highest level of each of our model 15-level LJ $(2n,n)$ potentials obtained using a given fixed mesh (in y), with the relative error $\delta_v^{h\to 0}$ obtained when $E_b(v)=E_b(v;h)$ in Eq. (35) is corrected by addition of the error term given by Eqs. (22) or (24). The two to five orders of magnitude error reduction from δ_v to $\delta_v^{h\to 0}$ attests to the validity and accuracy of the eigenvalue corrections yielded by these expressions. This provides a very straightforward way of greatly improving the accuracy of eigenvalues generated in the conventional way for a given finite mesh step length h.

As a final test case, we consider the model 301-level LJ (6,3) potential of the last row of Table I. It is representative of a class of molecular states of homonuclear alkali diatomic molecules which dissociate to n^2S+n^2P atoms, and are of considerable interest in the study of ultracold atoms and molecules. Two cases of this type are the $A^1\Sigma_u^+ \sim b^3\Pi_0$ systems of Li_2 [5] and K_2 [45]. The highest observed $A^1\Sigma_u^+$ state level for Li_2 is $v=92$ and $v=245$ for K_2, and calculations for these levels and predictions for higher ones are difficult to perform in the conventional r domain, as they have outer turning points $r_2(v) \gtrsim 90$ Å. The relative ease with which the new approach (see Table III) can treat such extremely weakly bound levels offers a remarkably straightforward method of addressing such problems.

For all levels of this 301-level model system, Fig. 7 shows the relative binding energy errors $\delta_v^{h\to 0}$ obtained using three different Numerov propagation cases and the PCM method. The more demanding $(N=5\times 10^4)$ Numerov application, which yields accuracy close to machine precision, only involves use of an average of ~200 grid points per loop of the wave function. Similarly, full convergence of the PCM and FCM methods for all levels of this potential is achieved with

TABLE II. Relative errors δ_v in the binding energies of the highest bound level of each of the 15-level model LJ $(2n,n)$ potentials of Table I obtained using the indicated optimized α value, total number of mesh points N, and numerical technique. For the finite difference (FD3) and propagation (Num) methods, $\delta_v^{h\to 0}$ was obtained with E_h replaced by $[E_h+\Delta E(h)]$ with $\Delta E(h)$ calculated from Eqs. (22) or (24). The numbers in parentheses indicate the power of 10 multiplying each associated number.

	FD3				Num				FCM		
n	N	α_{opt}	δ_v	$\delta_v^{h\to 0}$	N	α_{opt}	δ_v	$\delta_v^{h\to 0}$	N	α_{opt}	δ_v
6	20 000	1.36	8.1(−3)	3.6(−6)	5 000	1.07	1.1(−5)	1.0(−7)	200	0.66	2.5(−11)
5	20 000	1.26	2.5(−3)	1.5(−7)	2 000	1.00	8.2(−5)	1.7(−6)	200	0.55	1.1(−12)
4	20 000	1.06	5.3(−4)	4.8(−8)	2 000	0.88	9.1(−6)	3.5(−8)	180	0.51	6.3(−13)
3	20 000	0.63	1.6(−4)	8.0(−9)	2 000	0.57	1.0(−4)	1.6(−9)	150	0.31	1.3(−13)

TABLE III. Relative errors δ_v in the binding energy of the highest bound level of the 301-level model LJ (6, 3) potential of Table I obtained by the Numerov propagation method using $\alpha=\alpha_{\rm opt}=0.56$. $\delta_v^{h\to 0}$ values were obtained by replacing E_h by $[E_h+\Delta E(h)]$ where $\Delta E(h)$ was calculated from Eq. (24). Numbers in parentheses indicate the power of 10 multiplying each associated number, and N is the number of grid points.

N	δ_v	$\delta_v^{h\to 0}$
10000	3.3(−2)	3.3(−4)
20000	7.6(−4)	8.2(−6)
40000	4.7(−5)	1.1(−7)
60000	9.4(−6)	1.2(−8)

$N_{\rm coll}\lesssim 3\times v_{\rm last}$. In contrast, accurate treatment of the very highest levels of this potential using fix r-grid methods would require almost heroic degrees of computational effort using conventional methods.

The advantages of the present procedure will be somewhat smaller for potentials with $n=4$, 5, and 6, since the fact that the term C_n/r^n dies off more rapidly for large n means that relatively fewer levels will lie in the region very close to dissociation where the new method has most impact. At the same time, even for the $n=6$ case, performing practical calculations for the highest bound levels, which is completely routine for the present procedure, would be very challenging when using r as the radial variable.

In summary, the analytic coordinate mapping technique introduced here makes it very straightforward to solve the radial Schrödinger equation for levels lying extremely near dissociation which would be very difficult to treat using conventional methods based on the r domain. The much smaller numbers of integration mesh points N or collocation points $N_{\rm coll}$ associated with use of the present method also means that both computational effort and array storage requirements are substantially lower than with traditional r-coordinate calculations of equivalent accuracy. Moreover, the *analyticity* of the present mapping function eliminates the spurious (*ghost*) states which sometimes appear in the framework of numerical transformations implemented in Refs. [18,19]. For numerical integration methods, the present adaptive analytical mapping procedure completely avoids *termination* error, because inward integrations start (in principle) at the $r\to\infty$ limit, and it significantly reduces the effect of *truncation* error, because fewer integration mesh points are required.

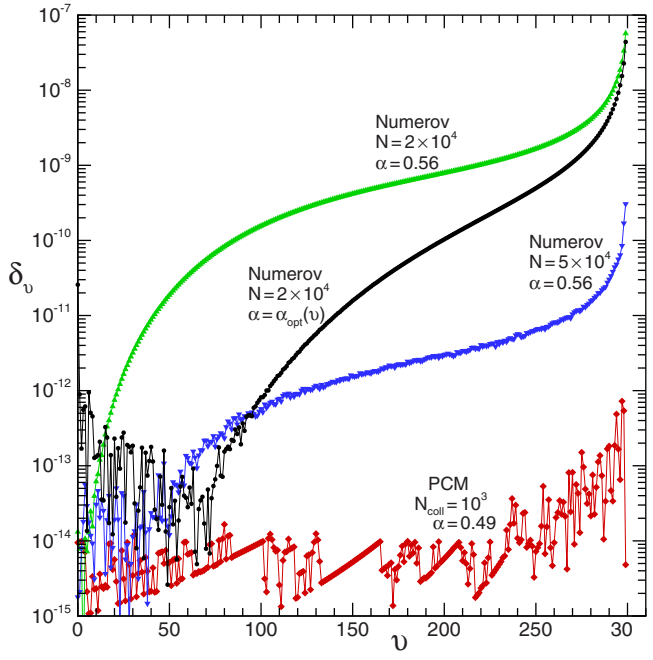

FIG. 7. (Color online) Relative errors of eigenvalues obtained by the polynomial collocation method (PCM) and by the Numerov propagation (Numerov) method extrapolated to zero step size ($\delta_v^{h\to 0}$), for vibrational levels $0\leqslant v\leqslant 299$ of the 301-level model LJ (6,3) system of Table I. N is the number of grid points.

In closing, we note that the advantages of having to deal with distinctly smaller numbers of radial integration steps will be of particular importance in applications of this approach to coupled-channel problems. Further work which shows that this approach also provides a particularly efficient and stable way of calculating photoassociation cross sections and scattering lengths and other zero-energy collision properties will be reported elsewhere [46].

ACKNOWLEDGMENTS

The authors are indebted to David Manolopoulos for fruitful and encouraging discussions in the early stage of this work, and A.V.S. is grateful to the Department of Chemistry of the University of Waterloo for its hospitality. This work has been supported by INTAS Grant No. 06-1000014-5964, by the Russian Foundation for Basic Researches (N06-03-32330a), and by NSERC Canada.

APPENDIX A: EIGENVALUE ERROR OF FINITE-DIFFERENCE METHOD

The conventional nth order finite-difference approximation of the second derivative term in Eq. (11) leads to the modified equation [26]

$$\left[-\frac{\hbar^2}{2\mu}\frac{d^2}{dy^2}+g^2\tilde{U}\right]\phi+R_n(h)=E_n(h)g^2\phi, \qquad \text{(A1)}$$

where the eigenfunction $\phi=\phi(y;h)$ coincides with finite-difference approximate eigenfunction at the grid points [10], and

$$R_n(h)=-c_n h^n\left(\frac{\hbar^2}{2\mu}\right)\phi^{(n+2)}+O(h^{n+2}), \qquad \text{(A2)}$$

$$\phi^{(n+2)}\equiv\frac{d^{n+2}\phi}{dy^{n+2}} \qquad \text{(A3)}$$

is the truncation error of the nth order scheme. The perturbative treatment of Eq. (A1) given first in Ref. [10] then allows one to represent the zeroth-order energy correction $E_n(h)=E_{h\to 0}(h)+\Delta E_n(h)+O(h^{n+2})$ by the closed form expression

$$\Delta E_n(h) = c_n h^n \left(\frac{\hbar^2}{2\mu}\right) \frac{\int_a^b \phi_0 \phi_0^{(n+2)} dy}{\int_a^b |g\phi_0|^2 dy}, \tag{A4}$$

where $\phi_0 = \phi + O(h^2)$ is the exact eigenfunction of Eq. (A1) corresponding to the eigenvalue $E_n(\mathrm{h} \to 0)$.

On integrating by parts in Eq. (A4) and making use of the differential equation (11) and the associated normalization condition of Eq. (13), we find that energy corrections for the central three-point (FD3) ($n=2$) and Numerov (Num) ($n=4$) schemes have the explicit forms

$$\Delta E_{\mathrm{FD3}} = \left(\frac{\hbar^2}{2\mu}\right) \frac{h^2}{12} \left[A_{\mathrm{FD3}} + \int_a^b (\tilde{Q}\phi)^2 dy \right], \tag{A5}$$

$$\Delta E_{\mathrm{Num}} = \left(\frac{\hbar^2}{2\mu}\right) \frac{h^4}{240} \left[A_{\mathrm{Num}} + \int_a^b \left(\frac{d(\tilde{Q}\phi)}{dy}\right)^2 dy \right], \tag{A6}$$

where

$$A_{FD3} = (\phi\phi^{(3)} - \phi^{(1)}\phi^{(2)})\big|_a^b = \phi^2 \tilde{Q}^{(1)}\big|_a^b, \tag{A7}$$

$$A_{\mathrm{Num}} = (\phi\phi^{(5)} - \phi^{(1)}\phi^{(4)} + \phi^{(2)}\phi^{(3)})\big|_a^b. \tag{A8}$$

When the effective potential $\tilde{U}(y)$ is nonsingular at the ends of the interval $[a,b]$ and the wave function $\phi(y)$ satisfies the standard boundary and normalization conditions (13), the A_{FD3} term vanishes and the A_{Num} term reduces to

$$A_{\mathrm{Num}} = -2[\phi^{(1)}]^2 \tilde{Q}^{(1)}\big|_a^b. \tag{A9}$$

APPENDIX B: PSEUDOSPECTRAL DIFFERENTIATION MATRICES

In the pseudospectral method of solving Eq. (11), the wave function is approximated by the interpolation function,

$$\phi(y) \approx \sum_{j=1}^{N_{\mathrm{coll}}} \phi(y_j) l_j(y), \tag{B1}$$

where $\{y_j\}$ are the collocation points and $\{l_j(y)\}$ are functions that have the property

$$l_j(y_i) = \begin{cases} 1, & i = j \\ 0, & i \neq j \end{cases}. \tag{B2}$$

Substituting Eq. (B1) into the Schrödinger equation of Eq. (11) using Eq. (B2) yields the generalized eigenvalue problem of Eq. (19) in which $\mathbf{A} = -(\hbar^2/2\mu)\mathbf{D^2} + \mathbf{V}$, $\mathbf{D^2}_{ij} = l_j''(y_i)$ is the matrix of second derivatives, and $\mathbf{V}_{ij} = g_i^2 \tilde{U}_i \delta_{ij}$ is the diagonal matrix of effective potential energy.

1. Polynomial collocation

The N_{coll} polynomial collocation points y_i are numerically defined as roots of the first derivatives of the Legendre polynomials, $dP_{N_{\mathrm{coll}}+1}/dy$,

$$l_j(y) = \left\{ \frac{y^2 - 1}{(N_{\mathrm{coll}} + 1)(N_{\mathrm{coll}} + 2) P_{N_{\mathrm{coll}}}(y_j)(y - y_j)} \right\} \times \frac{dP_{N_{\mathrm{coll}}}(y)}{dy} \tag{B3}$$

and

$$\mathbf{D}^2_{ij} = \begin{cases} \frac{1}{3} \frac{(N_{\mathrm{coll}} + 1)(N_{\mathrm{coll}} + 2)}{y_i^2 - 1}, & i = j \\ -\frac{2P_{N_{\mathrm{coll}}}(y_i)}{(y_i - y_j)^2 P_{N_{\mathrm{coll}}}(y_j)}, & i \neq j \end{cases}. \tag{B4}$$

While the matrix (B4) is nonsymmetric, the final matrix equation (21) can be symmetrized by the substitution $\varphi = \mathbf{C}\tilde{\varphi}$, where $\mathbf{C}$ is the diagonal matrix $C_{ii} = P_{N_{\mathrm{coll}}}(y_i)$.

2. Fourier collocation

The Fourier collocation points are $y_j = -1 + 2(j-1)/N_{\mathrm{coll}}$ for $j = 1, \ldots, N_{\mathrm{coll}}$ with N_{coll} odd, while

$$l_j(y) = \frac{1}{N_{\mathrm{coll}}} \frac{\sin[\pi N_{\mathrm{coll}}(y - y_j)/2]}{\sin[\pi(y - y_j)/2]} \tag{B5}$$

and

$$\mathbf{D}^2_{ij} = \begin{cases} \pi^2(1 - N_{\mathrm{coll}}{}^2)/12, & i = j \\ -(-1)^{i+j}\pi^2 \dfrac{\cos\left(\dfrac{\pi}{N_{\mathrm{coll}}}(i-j)\right)}{2\sin^2\left(\dfrac{\pi}{N_{\mathrm{coll}}}(i-j)\right)}, & i \neq j \end{cases}. \tag{B6}$$

The Fourier collocation method tacitly assumes periodic boundary conditions; however, it also works perfectly for wave functions which die off exponentially.

3. Sinc collocation

The Sinc collocation points are $y_j = -1 + jh$ where $h = 2/(N_{\mathrm{coll}} + 1)$ and $j = 1, \ldots, N_{\mathrm{coll}}$, while

$$l_j(y) = \frac{\sin[(\pi/h)(y - y_j)]}{(\pi/h)(y - y_j)} \tag{B7}$$

and

$$\mathbf{D}^2_{ij} = \begin{cases} -\pi^2/3h^2, & i = j \\ -2(-1)^{i+j}/h^2(i-j)^2, & i \neq j \end{cases}. \tag{B8}$$

Sinc collocation works perfectly for wave functions which die off exponentially.

[1] J. A. Coxon and P. G. Hajigeorgiou, Can. J. Phys. **70**, 40 (1992).

[2] J. Y. Seto, Z. Morbi, F. Charron, S. K. Lee, P. F. Bernath, and R. J. Le Roy, J. Chem. Phys. **110**, 11756 (1999).

[3] A. Pashov, W. Jastrzębski, and P. Kowalczyk, J. Chem. Phys. **113**, 6624 (2000).

[4] C. Samuelis, E. Tiesinga, T. Laue, M. Elbs, H. Knöckel, and E. Tiemann, Phys. Rev. A **63**, 012710 (2000).

[5] J. A. Coxon and T. C. Melville, J. Mol. Spectrosc. **235**, 235 (2006).

[6] J. W. Cooley, Math. Comput. **15**, 363 (1961).

[7] J. K. Cashion, J. Chem. Phys. **39**, 1872 (1963).

[8] P.-O. Löwdin, *An Elementary Iteration-Variation Procedure for Solving the Schrödinger Equation*, Technical Note No. 11, Quantum Chemistry Group, Uppsala University, Uppsala, Sweden, 1958.

[9] B. R. Johnson, J. Chem. Phys. **67**, 4086 (1977).

[10] H. C. Bolton and H. I. Scoins, Proc. Cambridge Philos. Soc. **52**, 215 (1956).

[11] D. G. Truhlar, J. Comput. Phys. **10**, 123 (1972).

[12] B. W. Shore, J. Chem. Phys. **59**, 6450 (1973).

[13] W. H. Press, S. A. Teukolsky, W. T. Vetterling, and B. P. Flannery, *Numerical Recipes in Fortran 77* (Cambridge University Press, Cambridge, U.K., 1999).

[14] J. P. Boyd, *Chebyshev and Fourier Spectral Methods*, 2nd Ed. (Dover Publications, Mineola, NY, 2000).

[15] R. Meyer, J. Chem. Phys. **52**, 2053 (1970).

[16] V. Kokoouline, O. Dulieu, and R. Kosloff, J. Chem. Phys. **110**, 9865 (1999).

[17] F. Masnou-Seeuws and P. Pillet, Adv. At., Mol., Opt. Phys. **47**, 53 (2001).

[18] K. Willner, O. Dulieu, and F. Masnou-Seeuws, J. Chem. Phys. **120**, 548 (2004).

[19] M. Nest and H.-D. Meyer, Chem. Phys. Lett. **352**, 486 (2002).

[20] J. P. Boyd, C. Rangan, and P. H. Bucksbaum, J. Comput. Phys. **188**, 56 (2003).

[21] S. Kallush and R. Kosloff, Chem. Phys. Lett. **433**, 221 (2006).

[22] J. Liouville, J. Math. Pures Appl. **2**, 16 (1837); G. Green, Trans. Cambridge Philos. Soc. **6**, 457 (1837).

[23] L. D. Landau and E. M. Lifshitz, *Quantum Mechanics* (Pergamon, New York, 1965).

[24] M. S. Child, *Semiclassical Mechanics with Molecular Applications* (Clarendon Press, Oxford, 1991).

[25] R. J. Le Roy, LEVEL 8.0: *A Computer Program for Solving the Radial Schrödinger Equation for Bound and Quasibound Levels*, University of Waterloo Chemical Physics Research Report CP-663, 2007, see http://leroy.uwaterloo.ca/programs/

[26] Note that throughout this paper the symbol h represents mesh step size, while $\hbar$ is Planck's constant divided by 2π.

[27] A. A. Šurkus, R. J. Rakauskas, and A. B. Bolotin, Chem. Phys. Lett. **105**, 291 (1984).

[28] R. J. Le Roy and Y. Huang, J. Mol. Struct.: THEOCHEM **591**, 175 (2002).

[29] Y. Huang and R. J. Le Roy, J. Chem. Phys. **119**, 7398 (2003); **126**, 169904(E) (2007).

[30] R. J. Le Roy, D. R. T. Appadoo, K. Anderson, A. Shayesteh, I. E. Gordon, and P. F. Bernath, J. Chem. Phys. **123**, 204304 (2005).

[31] R. J. Le Roy, Y. Huang, and C. Jary, J. Chem. Phys. **125**, 164310 (2006).

[32] Three such forms are $y(r)=1-\exp[-\alpha r^{\gamma}]$, $y(r)=\exp\{-\exp[\alpha(r-\bar{r})]\}$, and the function $y(r;\alpha,\bar{r}>0)=\arctan[\alpha(r-\bar{r})]$ for which $r(y)=\bar{r}+\tan(y)/\alpha$ with $y\in[\arctan(-\alpha\bar{r}),\pi/2]$. For this last case $g(y)=1/\{\alpha\cos^2(y)\}=\{1+[\alpha(r-\bar{r})]^2\}/\alpha$ and the function $F(y)=1$.

[33] H. Margenau, Rev. Mod. Phys. **11**, 1 (1939).

[34] J. O. Hirschfelder, C. F. Curtiss, and R. B. Bird, *Molecular Theory of Gases and Liquids* (Wiley, New York, 1964).

[35] J. O. Hirschfelder and W. J. Meath, Intermolecular Forces, Vol. 12 of Adv. Chem. Phys., edited by J. O. Hirschfelder (Interscience, New York, 1967), pp. 3–106.

[36] A summary of rules determining the limiting value of n for any particular case may be found in Refs. [37–39].

[37] R. J. Le Roy and R. B. Bernstein, J. Chem. Phys. **52**, 3869 (1970).

[38] W. J. Meath, Am. J. Phys. **40**, 21 (1972).

[39] R. J. Le Roy, in *Molecular Spectroscopy*, edited by R. Barrow, D. A. Long, and D. J. Millen (Chemical Society of London, London, 1973), Vol. 1, Specialist Periodical Report 3, pp. 113–176.

[40] For our collocation method calculations, the ordinary eigenvalue problem of the resulting symmetric matrix (21) was solved by the implicitly restarted Lanczos method taken in the shift-inverted spectral transformation mode [41].

[41] R. B. Lenoucq, D. C. Sorensen, and C. Yang, *ARPACK User's Guide: Solution of Large Scale Eigenvalue Problems with Implicitly Restarted Arnoldi Methods* (SIAM, Philadelphia, PA, 1998).

[42] R. J. Le Roy and R. B. Bernstein, J. Chem. Phys. **54**, 5114 (1971).

[43] R. J. Le Roy and W.-K. Liu, J. Chem. Phys. **69**, 3622 (1978).

[44] J. M. Hutson, J. Phys. B **14**, 851 (1981); J. M. Hutson, QCPE Bulletin 2, No. 2, Program #435, Quantum Chemistry Program Exchange, Indiana University, Bloomington, Indiana.

[45] St. Falke, I. Sherstov, E. Tiemann, and Ch. Lisdat, J. Chem. Phys. **125**, 224303 (2006).

[46] R. J. Le Roy, V. V. Meshkov, and A. V. Stolyarov (unpublished).